ORNL-3823
UC-33 – Propulsion Systems and
Energy Conversion
TID-4500 (41st ed.)

NASA Order No. C-220-A
(Interagency Agreement 40-14-63)

SNAP-8 CORROSION PROGRAM

QUARTERLY PROGRESS REPORT

FOR PERIOD ENDING FEBRUARY 28, 1965

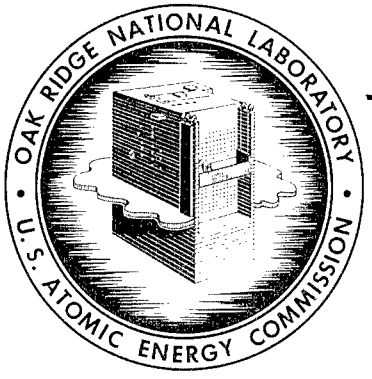

OAK RIDGE NATIONAL LABORATORY
operated by
UNION CARBIDE CORPORATION
for the
U.S. ATOMIC ENERGY COMMISSION

Printed in USA. Price $3.00. Available from the Clearinghouse for Federal Scientific and Technical Information, National Bureau of Standards, U.S. Department of Commerce, Springfield, Virginia

ORNL-3823

Contract No. W-7405-eng-26

NASA Order No. C-220-A
(Interagency Agreement 40-14-63)

SNAP-8 CORROSION PROGRAM
QUARTERLY PROGRESS REPORT
For Period Ending February 28, 1965

H. W. Savage
E. L. Compere
R. E. MacPherson
W. R. Huntley
A. Taboada

JUNE 1965

OAK RIDGE NATIONAL LABORATORY
Oak Ridge, Tennessee
operated by
UNION CARBIDE CORPORATION
for the
U.S. ATOMIC ENERGY COMMISSION

CONTENTS

SNAP-8 CORROSION PROGRAM QUARTERLY PROGRESS REPORT FOR PERIOD ENDING FEBRUARY 28, 1965

INTRODUCTION

A corrosion-study program was initiated in June 1963 at the Oak Ridge National Laboratory in support of the SNAP-8 electrical generating system. The primary objectives of the program are (1) to evaluate the compatibility of the proposed structural materials with the proposed reactor coolant, NaK containing hydrogen, and (2) to provide information on the behavior, control, and disposition of the hydrogen present in the SNAP-8 primary coolant, particularly with respect to the diffusion of hydrogen from the SNAP-8 primary circuit through Croloy 9M boiler tubes into the power conversion circuit.

The program initially provided for 12 loop experiments, with time and space available in the schedule for a thirteenth loop. The 12 initial experiments included the operation of eight loops to obtain information for a factorial replicate study of three variables at two levels each, two loops for a time-series study at SNAP-8 conditions, and two (or three) additional loops for investigating means of limiting hydrogen egress through the Croloy 9M cooler section of the loop. In addition, the program included a study of hydrogen permeability for three SNAP-8 container materials with and without NaK present and an investigation of the relationships between hydrogen solubility and partial pressure in NaK as a function of temperature.

Several modifications have been made to the original loop program. Three "hot-spot" loops have been added; in each of these a redesigned hot section more closely simulates the SNAP-8 hot-spot condition than was achievable with the loops as originally designed. Two of these loops are also being used to study hydrogen egress and control. Four of the original loops (see Table 1) and one of the hot spot loops were deferred pending a more complete evaluation of the results from the existing loops.

Previous reports[1-6] in this series described in detail the program plan, the experiments to be conducted, and the test equipment to be used to simulate the SNAP-8 primary circuit at reduced scale. Startup and operating experience for ten loops, including the first hot-spot loop, were also described, including the difficulties encountered in maintaining and measuring oxygen and hydrogen levels in the NaK. Ten loops have completed operation to date. Cold trapping has been effective in controlling contaminants and has reduced hydrogen effluent from the loops at cold trap temperatures as high as 250°F. Plug indicators used to determine oxide levels in the loops have consistently shown multiple responses, indicating the presence of contaminants other than Na_2O. Sampling devices for isolating the other contaminants have shown only K_2O and Na_2O and no evidence of corrosion products or carbon compounds. Characterization of the behavior of hydrogen in the loops is being studied in the light of the discovery of extraneous sources of hydrogen, and monitoring of loop hydrogen effluents is being revised to overcome deficiencies found in the argon-sweep-gas and thermal-conductivity-cell technique used to date.

Procedures for postrun examination of corrosion loops were developed, and results from the examination of completed loop experiments showed some degree of corrosion and mass transfer in each loop. Low-oxygen-content loops had very little corrosion, but high-oxygen-content loops had significantly greater amounts. The oxygen level was shown to have a greater

---

[1]H. W. Savage et al., SNAP-8 Corrosion Program Quart. Progr. Rept. Aug. 31, 1963, USAEC Report ORNL-3538, Oak Ridge National Laboratory.

[2]H. W. Savage et al., SNAP-8 Corrosion Program Quart. Progr. Rept. Nov. 30, 1963, USAEC Report ORNL-3604, Oak Ridge National Laboratory.

[3]H. W. Savage et al., SNAP-8 Corrosion Program Quart. Progr. Rept. Feb. 29, 1964, USAEC Report ORNL-3618, Oak Ridge National Laboratory.

[4]H. W. Savage et al., SNAP-8 Corrosion Program Quart. Progr. Rept. May 31, 1964, USAEC Report ORNL-3671, Oak Ridge National Laboratory.

[5]H. W. Savage et al., SNAP-8 Corrosion Program Quart. Progr. Rept. Aug. 31, 1964, USAEC Report ORNL-3730, Oak Ridge National Laboratory.

[6]H. W. Savage et al., SNAP-8 Corrosion Program Quart. Progr. Rept. Nov. 30, 1964, USAEC Report ORNL-3784, Oak Ridge National Laboratory.

effect on the corrosion of iron-base alloys than on that of nickel-base alloys. Carbon migration has been severe in all loops and is apparently independent of the oxygen content of the NaK at the oxygen levels investigated. Extensive decarburization was observed in the hot sections of the Croloy 9M, and, in some cases, the decarburization was accompanied by large grain growth. Carbon pickup was observed throughout the rest of the loop. Hydrogen at the low levels experienced in the loops does not adversely affect corrosion and mass transfer.

It was found that chromium enrichments of the surfaces of chromized Hastelloy N piping and tubing typical of SNAP-8 fuel element cladding vary in a random fashion from 0 to 75% chromium and to a maximum depth of 0.0015 in. Such variation is not expected to have a significant effect on corrosion.

Hydrogen permeability of Hastelloy N was measured both in the presence and absence of NaK and of type 316 stainless steel and Croloy 9M in the absence of NaK, as reported previously. Also an equation for the solubility of hydrogen in NaK was determined:

$$\log_{10} \frac{X}{P^{1/2}} = 0.0756 + \frac{274}{T},$$

where

X = hydrogen concentration, cc (STP) per g of NaK,

P = hydrogen partial pressure, atm,

T = temperature, °K.

In the absence of cold trapping, the hydrogen partial pressure in the SNAP-8 primary NaK system at 1100°F should be about 2.4×10^{-5} atm. Cold trapping at about 100°F would be needed to reduce this concentration by a factor of 10^4 and the hydrogen diffusion through the Croloy 9M by a factor of 10^2. Solid getters for hydrogen, such as zirconium or yttrium, might also effect a similar reduction in concentration, but use of a soluble getter, such as lithium, accompanied by cold trapping at temperatures around 300°F appears to have the most promise of effective hydrogen control. Diffusion windows appear to be impractical.

This report covers progress during the seventh quarterly period of the program, December 1, 1964 to February 28, 1965.

SUMMARY

Installation and shakedown operation of the second hot-spot loop (14-4) were completed during this reporting period. While identical in basic configuration with the hot-spot loop already tested (loop 13-3), it will be operated with continuous cold trapping to observe differences in corrosion and mass transfer rates and to evaluate the effectiveness of cold trapping in reducing the hydrogen concentration in the loop NaK and thus the hydrogen effluent from the loop. Two hydride cold traps are provided, one for the collection of hydrogen from extraneous sources while no hydrogen is being deliberately injected into the loop and the other for the collection of hydrogen during normal hydrogen injection. Deuterium is to be substituted for hydrogen to permit characterization of the behavior of hydrogen in the SNAP-8 primary circuit independently of effects of hydrogen from extraneous sources.

During this reporting period loop 14-4 operated 1027 hr at design temperature and the hydride trap for collecting extraneous hydrogen operated 248 hr. Extraneous hydrogen was observed with the use of both gas-sampling techniques and an on-stream mass spectrometer; however, the rate of extraneous hydrogen flow diminished with time. A study of the multibreak curves from the oxide plugging indicator revealed that the first (highest temperature) break was caused by argon cover gas coming out of solution during cooling to form a liquid-gas mixture that markedly reduced flow through the indicator orifices. The second break was caused by an unknown material that apparently is not an oxide.

Results of analytical examinations of the corrosion loops during this period in general confirmed previous observations. Very little metal migration occurred in low-oxygen-content NaK at both temperature levels investigated; however, carbon migration was quite severe. Corrosion of the iron-base alloys in the low-oxygen-content NaK was very low, as compared with corrosion of the chromized Hastelloy N, which

ranged from three to seven times as great. Increasing the oxygen content of the NaK accelerated the corrosion rate on all materials; however, the effect on the corrosion rate of Hastelloy N was much less than that experienced by iron-base alloys. High corrosion rates were observed in some loops run with low oxide content. The results observed would be consistent with a hypothesis that intermittent high oxide situations in an otherwise low oxide regime are as damaging as continuous high oxide contents. Additions of hydrogen to the NaK did not produce any discernible effects on the mass transfer rates. Furthermore, the extent of carbon migration apparently was not affected by hydrogen or oxygen levels in the NaK.

Because of the extensive decarburization of Croloy 9M in the SNAP-8 corrosion loops, a study was made for determining the effects of decarburization on selected mechanical properties. Sheet tensile specimens were decarburized to a carbon content of approximately 0.002 to 0.01% by exposure to NaK in a forced-flow type 316 stainless steel loop. A general deterioration of mechanical properties was observed.

Studies were conducted of the permeation of hydrogen and deuterium through type 316 stainless steel in the presence of NaK. The ratio of permeability of deuterium and hydrogen was 0.68 at 1100°F and 0.74 at 1300°F; these values compare favorably with the anticipated ratio of 0.71. Permeation of hydrogen through a type 316 stainless steel diaphragm was appreciably reduced by exposing the stainless steel to air for short periods. The passage of hydrogen through the diaphragm eventually removed the oxide layer formed and restored the permeation rate.

Hydrogen solubilities in NaK-78 were determined for a temperature range of 572 to 1300°F as a function of hydrogen pressure from a few millimeters to 1 atm, and Sievert's law was found to hold for this system. Evidence of solid hydride precipitation was observed below 752°F. For estimated hydrogen pressures in the SNAP-8 primary coolant, these data indicate a hydrogen concentration in the NaK of 1 ppm and precipitations of solid hydrides at approximately 300°F.

Studies of the phase equilibria of the Na-K-Li-H system at 1100°F indicate that in all cases examined the addition of lithium greatly lowers the partial pressure of hydrogen at equivalent hydrogen concentrations. This is apparently due to the hydrogen combining with the

respective alkali metals in proportion to their concentration and affinity for hydrogen. The limited solubility of lithium hydride results in precipitation, which inhibits pressure changes until the available lithium is exhausted.

FORCED-FLOW CORROSION-LOOP EXPERIMENTS

W. R. Huntley R. E. MacPherson
B. Fleischer A. Taboada

General Status

The status of all corrosion loop experiments proposed and operated to date is given in Table 1, and pertinent operating conditions of each loop are described. Fabrication and operation of loop 15 was deferred indefinitely. Loop 15 was to have been essentially a bimetallic loop of type 316 stainless steel and Chromized Hastelloy N that would have simulated the primary circuit for a SNAP-8 system that employed Croloy 9M–type 316 stainless steel duplex tubing for the mercury boiler.

Fabrication

Fabrication of loop 14-4 was completed and the loop was charged with NaK on December 17. Construction is 90% complete on a second isothermal (1425°F) type 316 stainless steel loop, which will be used to decarburize specimens of standard Croloy 9M and modified Croloy 9M alloy.

Operation

Loop 14-4

Loop 14-4 is the second hot-spot loop to be operated. It is similar to previously operated loop 13-3 except that continuous cold trapping is being employed in loop 14-4 to permit observation of differences in corrosion and mass transfer that may result and to evaluate the effectiveness of cold trapping in reducing the hydrogen level of the SNAP-8 primary system. Two hydride cold traps are provided in addition to a larger cold

Table 1. Status of All Proposed and Operated Forced-Convection Loops

Loop and Stand Nos.	Planned Operating Time (hr)	Maximum NaK Temperature (°F)	Oxygen Content of NaK (ppm)	Hydrogen Content of NaK	Variables To Be Studied	Comparison Loop	Time of Operation At Design Conditions (hr)	Status As of February 28, 1965
1-1	2000	1400	<30	0	Temperature	1A, 10	701[a]	Complete
					Oxygen content	2		
					Hydrogen content	4		
1A-1	2000	1400	<30	0	Temperature	10	2003	Complete
					Oxygen content	2		
					Hydrogen content	4		
2-2	2000	1400	~80	0	Temperature	9	2004	Complete
					Oxygen content	1		
					Hydrogen content	3		
3[b]	2000	1400	~80	SNAP-8[c]	Temperature	7	0	Deferred[b]
					Oxygen content	4, 6		
					Hydrogen content	2		
4-4	2000	1400	<30	SNAP-8	Temperature	8	2033	Complete
					Oxygen content	3, 6		
					Hydrogen content	1A, 1		
5-5	6000	1400	SNAP-8[d]	SNAP-8	Operating time	6	5133	Complete
6[b]	2000	1400	SNAP-8	SNAP-8	Operating time	5	0	Deferred[b]
					Oxygen content	3, 4		
					Hydrogen content	11, 12		
7-3	2000	1300	~80	SNAP-8	Temperature	3	2021	Complete
					Oxygen content	8		
					Hydrogen content	9		
8-4	2000	1300	<30	SNAP-8	Temperature	4	2053	Complete
					Oxygen content	7		
					Hydrogen content	10		
9-2	2000	1300	~80	0	Temperature	2	2000	Complete
					Oxygen content	10		
					Hydrogen content	7		
10-1	2000	1300	<30	0	Temperature	10	2000	Complete
					Oxygen content	9		
					Hydrogen content	8		
11[b]	2000	1400	SNAP-8	SNAP-8	Hydrogen content	6, 12	0	Deferred[b]
12[b]	2000	1400	SNAP-8	SNAP-8	Hydrogen content	6, 11	0	Deferred[b]
13-3	2000	1450	SNAP-8	SNAP-8	Hot spot	6	2000	Examination in progress
14-4	2000	1450	~30	Low	Continuous cold trapping	13	1027	In operation
15	2000	1450	SNAP-8	SNAP-8	No Croloy 9M in system	14, 13	0	Deferred

[a] Run completed.

[b] See ref. 5, p. 7.

[c] The entry SNAP-8 indicates that the hydrogen content is that expected in the full-scale SNAP-8 system.

[d] The entry SNAP-8 indicates an oxygen level simulating that of the full-scale SNAP-8 system with initial oxygen removal from the NaK and no further oxygen trapping during operation.

trap, which was used for initial loop oxide removal. One hydride trap is presently being operated on a 500-hr test for collection of hydrogen from extraneous sources, such as the atmosphere, the loop metals, and the NaK. A second hydride trap will be used for collection of deuteride while deuterium is being injected into the loop in lieu of the normal hydrogen injection. Deuterium is to be substituted to permit differentiation between extraneous hydrogen sources and the intentional injections into the loop.

Hydrogen and deuterium diffusion from the loop into an evacuated annulus will be monitored with a mass spectrometer. Measurements will be taken with and without cold trapping to obtain a measure of cold trapping performance. The design of the loop was covered in detail in a previous progress report.[7]

At the close of this quarter, the loop had accumulated 779 hr at design temperature during various shakedown operations plus 248 hr at design conditions with one of the hydride traps in operation for collection of extraneous hydrogen.

Argon Gas Transfer in Loop 14-4 Due to Differential Temperature Solubility in NaK

The economizer in the oxide-removal bypass system of loop 14-4 and the vertical pipe runs leading to it (see Fig. 1) have provided volumes where gas may be trapped; these did not exist in previous loops. During shakedown operation, this piping configuration served as a means for observing the rate at which argon could be transferred by differential temperature solubility from the flow-through surge tank through the NaK to cooler regions. Some gas transfer was noted on all previous loops as variations in the liquid level at the surge tank, but these variations were much smaller than in loop 14-4 due to different bypass piping configurations. Loop 14-4 was vacuum filled originally and was free of trapped gas as observed by varying the loop pressure from 2 to 20 psig with no indicated level change at the surge tank. After a few hours of

---

[7]W. R. Huntley et al., Forced-Flow Corrosion-Loop Experiments, p. 8, SNAP-8 Corrosion Program Quart. Progr. Rept. Nov. 30, 1964, USAEC Report ORNL-3784, Oak Ridge National Laboratory.

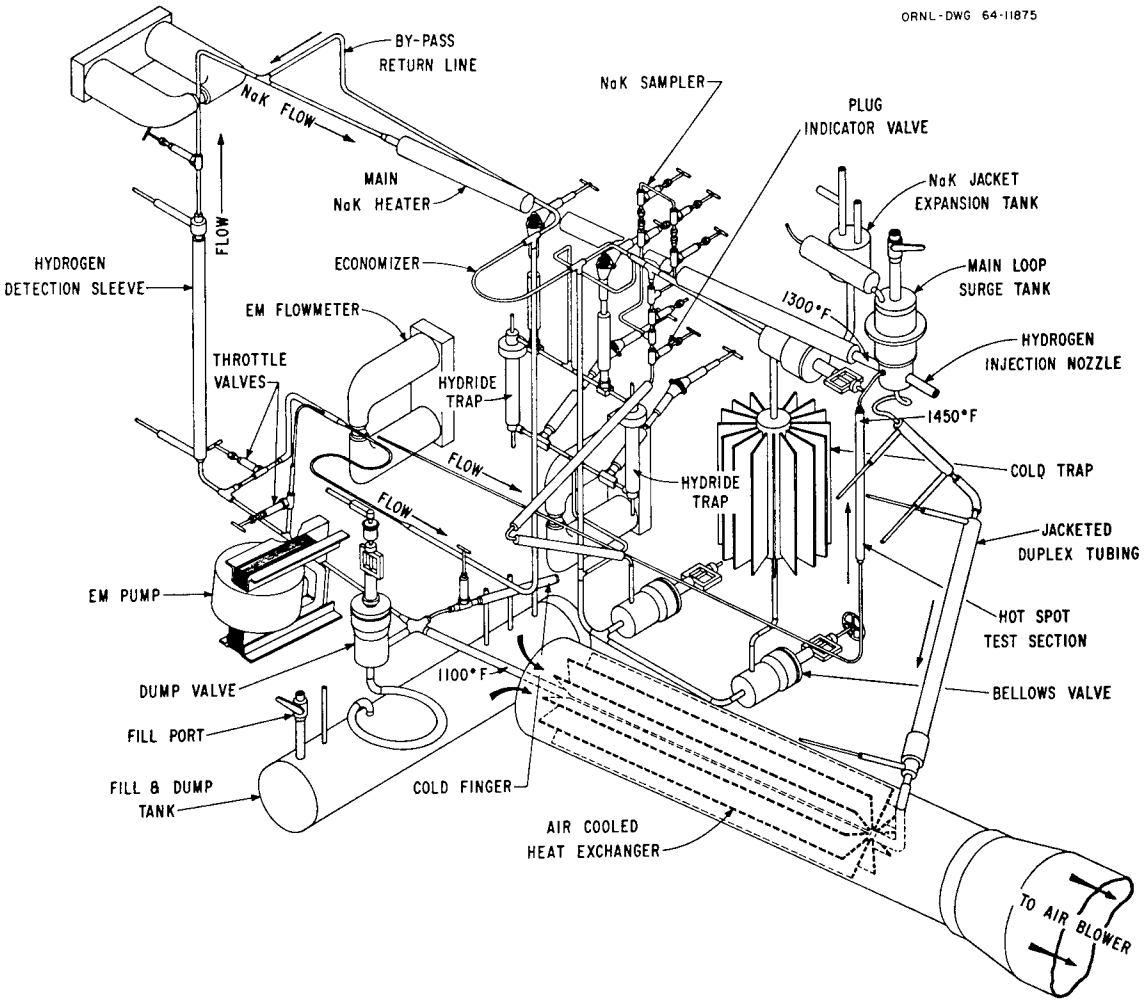

Fig. 1. Isometric Drawing of Loop 14-4.

operation at temperature, the system was observed to be "soft" in that the NaK liquid level would vary with changes in cover gas pressure.

A test was run to show that the rate of argon transfer into the trapping areas of the bypass system was proportional to the temperature difference in the NaK. This was done to demonstrate that gas was being transferred by solubility and not by simple gas entrainment at the flow-through surge tank. The first run was made with 10 psig of argon cover gas on the surge tank with a bypass flow rate of 0.07 gpm and with a 200°F temperature difference between the surge tank surface and the bypass exit. The gas accumulation was observed by a gradual increase of the surge tank

level as the argon collected in the trapped volumes of the bypass, and it was calculated to be 0.2 $in.^3$ (STP) of argon per hour. The second run was made with the same cover gas pressure and NaK flow rate, but with a 1100°F temperature difference between the surge tank surface and the bypass exit, and the gas accumulated at a rate of 1.5 $in.^3$ (STP) of argon per hour, or about seven times as fast.

A further test was made to establish that the gas accumulating in the cooled regions of the bypass system was indeed argon. NaK flow was directed through the bypass NaK sampler and through a valved sample bomb containing an enlarged cross section for gas accumulation. The bomb was evacuated at room temperature, filled with NaK by opening isolation valves leading to the loop, and then x-rayed to determine the degree of filling. While the loop was operating at design conditions, NaK at 1100°F was directed isothermally through the bypass and bomb for 30 min at 0.1 gpm. The flow was then blocked by the inlet valve, and the bomb was cooled to room temperature. A second x-ray showed that no noticeable amount of gas had accumulated. Flow was restarted through the bomb for 30 min at 0.1 gpm, with the NaK being cooled from 1100 to 200°F. Flow was again stopped, and a third x-ray showed that the enlarged portion of the bomb had filled with gas. The bomb was removed from the loop and the mass spectrometer analysis of the gas trapped above the NaK surface within the bomb was as follows:

Gas	Volume (%)
A	98.9
O_2	0.008
N_2 + CO	0.88
H_2O	0.12
H_2	0.05

Extraneous Hydrogen Measurements on Loop 14-4

Three sets of gas samples were removed over a 13-day period from the hydrogen detection annuli of loop 14-4 for mass spectrometer analysis. The analytical results are presented in Table 2. The sampling was done prior to the attachment of the on-line mass spectrometer to the loop and

Table 2. Hydrogen Content of Argon Effluent from Loop 14-4 Detection Annuli[a]

Argon flow rate through annuli: 25 cc/min

Date of Sampling	Hydrogen Content of Argon Entering Annuli (ppm)	Sampling Point 1[b]			Sampling Point 2[c]			Sampling Point 3[d]			Sampling Point 4[e]		
		Purge Time (hr)	Hydrogen Content (ppm)		Purge Time (hr)	Hydrogen Content (ppm)		Purge Time (hr)	Hydrogen Content (ppm)		Purge Time (hr)	Hydrogen Content (ppm)	
			Mass Spectrometer Result	Thermal Conductivity Cell Reading		Mass Spectrometer Result	Thermal Conductivity Cell Reading		Mass Spectrometer Result	Thermal Conductivity Cell Reading		Mass Spectrometer Result	Thermal Conductivity Cell Reading
1-21-65[f]	10	1/2	18	28	3 1/2	13	11	1/2	50	42	3 1/2	18	20
1-28-65[g]	7	1/2	27	19	3 1/2	11	7	15	16	12	16 1/2	11	7
2-4-65[g]	7	3	12	10	4 1/2	11	7	15	13	12	16 1/2	14	7

[a] All concentrations are ppm by volume. All samples were taken in 1, 2, 3, and 4 sequence of sampling points. Points 1 and 2 are on a common header, and points 3 and 4 are on a common header. Loop was at design temperature with no deuterium injection into loop prior to sampling. The thermal-conductivity cell readings have been corrected by adding the hydrogen content of the inlet argon to the output reading.

[b] Type 316 stainless steel wall.

[c] Croloy 9M–type 316 stainless steel duplex tubing wall.

[d] Croloy-9M wall.

[e] Type 316 stainless steel wall.

[f] Cold trap isolated three days before sampling.

[g] Samples taken while cold trapping at 260°F.

prior to the injection of deuterium into the NaK stream. During the 13-day sampling period, argon gas of known hydrogen content (7–10 ppm) was flowing through each of the four purge annuli at the rate of 25 cc/min. In addition to the gas sampling, the effluent argon stream was monitored for hydrogen by means of the standard thermal-conductivity apparatus available at the test facility.

The samples were taken for comparison with a similar set from loop 13-3 which had shown hydrogen concentrations of about 30 ppm. Any pickup of hydrogen was unexpected and could not be easily explained.

Initial measurements of hydrogen concentration in the loop 14-4 gas samples ranged from 13 to 50 ppm. It was found that more consistent results were obtained by maintaining the same argon flow rate of 25 cc/min and increasing the purge time through the sampling header and sample bomb from the normal 30 min to a minimum of 3 hr. With this procedure the hydrogen content of the effluent purge gas was normally in the range of 11 to 16 ppm and in good agreement with the measurements made with the recently recalibrated thermal-conductivity instrument. It was concluded that earlier data from loop 13-3 were in error due to insufficient purging of the sampling apparatus prior to taking the gas samples.

The source of hydrogen for the loop 14-4 samples that increased the hydrogen content of the argon to above the inlet value is not known. The moisture content of the argon has been periodically checked with an on-stream monitor downstream of the molecular sieve in the gas supply train and has consistently shown water vapor contents of about 1 ppm. This is consistent with the values shown by the mass spectrometer analysis of the gas in each argon cylinder prior to use and would appear to rule out water vapor in the argon supply as a major source of H_2 in the effluent from the high-temperature annuli.

After 635 hr of loop operation at design temperatures, during which continual argon flow had been maintained at 25 cc/min through the detection annuli, the loop was shut down on February 9 for attachment of the mass spectrometer to annulus No. 2. This 23-in.-long annulus is normally operated at about 1270°F and has a NaK containment wall of 0.050-in.-thick Croloy 9M–type 316 stainless steel duplex tubing through which

hydrogen diffuses from the loop NaK. The mass spectrometer has been adjusted to monitor masses 2, 3, and 4 and can be calibrated with standard leaks of H_2, HD, and D_2 attached to the apparatus by suitable valving. The purge flow of argon in the remaining three annuli was stopped to provide only a static inert atmosphere on these annuli for the remainder of the operation. The flow of argon through the annuli was stopped to preclude supplying hydrogen to the loop from the residual hydrogen in the argon, which usually is in the 6 to 20 ppm (by volume) range.

Measurable amounts of hydrogen were observed by the mass spectrometer when the loop was brought up to temperature with no hydrogen injection into the loop and with the cold trap operating continuously at 260°F. Initial values of hydrogen flow from the annulus averaged approximately 10×10^{-6} cc (STP)/sec and gradually lowered to an average of approximately 3×10^{-6} cc (STP)/sec in a 13-day period. During this period the hydrogen flow rate from the annulus was also observed with the loop cooled to room temperature and was found to be at least a factor of a thousand less [$<10^{-8}$ cc (STP)/sec]. The higher hydrogen flow rate returned when the loop was reheated to design temperature. The background levels of HD and D_2 from the annulus were also measured and were found to be much less [10^{-7}–10^{-8} cc (STP)/sec] than the hydrogen flow, as would be expected prior to D_2 injection into the NaK. It is concluded from the measurements taken to date that the mass spectrometer system will have adequate sensitivity and stability to monitor the higher flow rates of HD and D_2 that will be encountered during later phases of test loop operation when deuterium is intentionally injected.

Multibreak Oxide Plugging Indicator Studies

Observations of multiple breaks in flow through the plugging indicator have been made throughout this corrosion study program. The first observations reported[8] were for loop 10-1, where indications of a precipitate other than oxide was noted at plugging indicator temperatures of 400

[8]W. R. Huntley et al., Forced-Flow Corrosion-Loop Experiments, p. 7, SNAP-8 Corrosion Program Quart. Progr. Rept. Feb. 29, 1964, USAEC Report ORNL-3618, Oak Ridge National Laboratory.

to 500°F. This precipitate could not be completely removed by cold trapping at temperatures as low as 100°F, but the initial point of precipitation could usually be lowered to a plugging indicator temperature of about 300°F. If no further trapping was employed, this break point would increase again in two to four days to levels between 400 and 500°F. At lower temperatures a second and more rapid break in flow was observed that was consistent with cold-trapping temperatures and presumably reflected the oxide level. This oxide break could be eliminated completely in loop 10-1 (and all subsequent loops) by cold trapping at low temperatures. The absence of a break in the flow curve corresponding to these low cold-trap temperatures is due to insufficient oxygen being available in the limited NaK volume (115 $in.^3$) of the loops to form a plug.

In later loops of higher oxide content (loops 9-2 and 7-3), it was normal to preheat the plugging indicator to higher temperatures than those of loop 10-1 (1100 to 1200°F) prior to the plugging indicator cooling run. In these two loops an additional break in the plugging-indicator flow rate was observed in the range from 800 to 1100°F. This preheat procedure was adopted as a standard technique and was applied to all subsequent plugging runs. Throughout the course of the test program, two breaks consistently continued to occur at levels above the oxide break and above the cold-trap operating temperature. A typical three-break plugging indicator trace is shown in Fig. 2.

Observations of the initial plugging break (800 to 1100°F) were reported earlier.[9,10] A brief summary of the previous observations and of the more recent experience follows:

1. In a new system the initial break occurs in the temperature range 900 to 1100°F.

2. Random variations of ±100°F are observed in the initial break temperature after cold trapping at temperatures as low as 110°F.

---

[9]W. R. Huntley et al., Forced-Flow Corrosion-Loop Experiments, p. 6, SNAP-8 Corrosion Program Quart. Progr. Rept. May 31, 1964, USAEC Report ORNL-3671, Oak Ridge National Laboratory.

[10]Op. cit., ref. 7, p. 17.

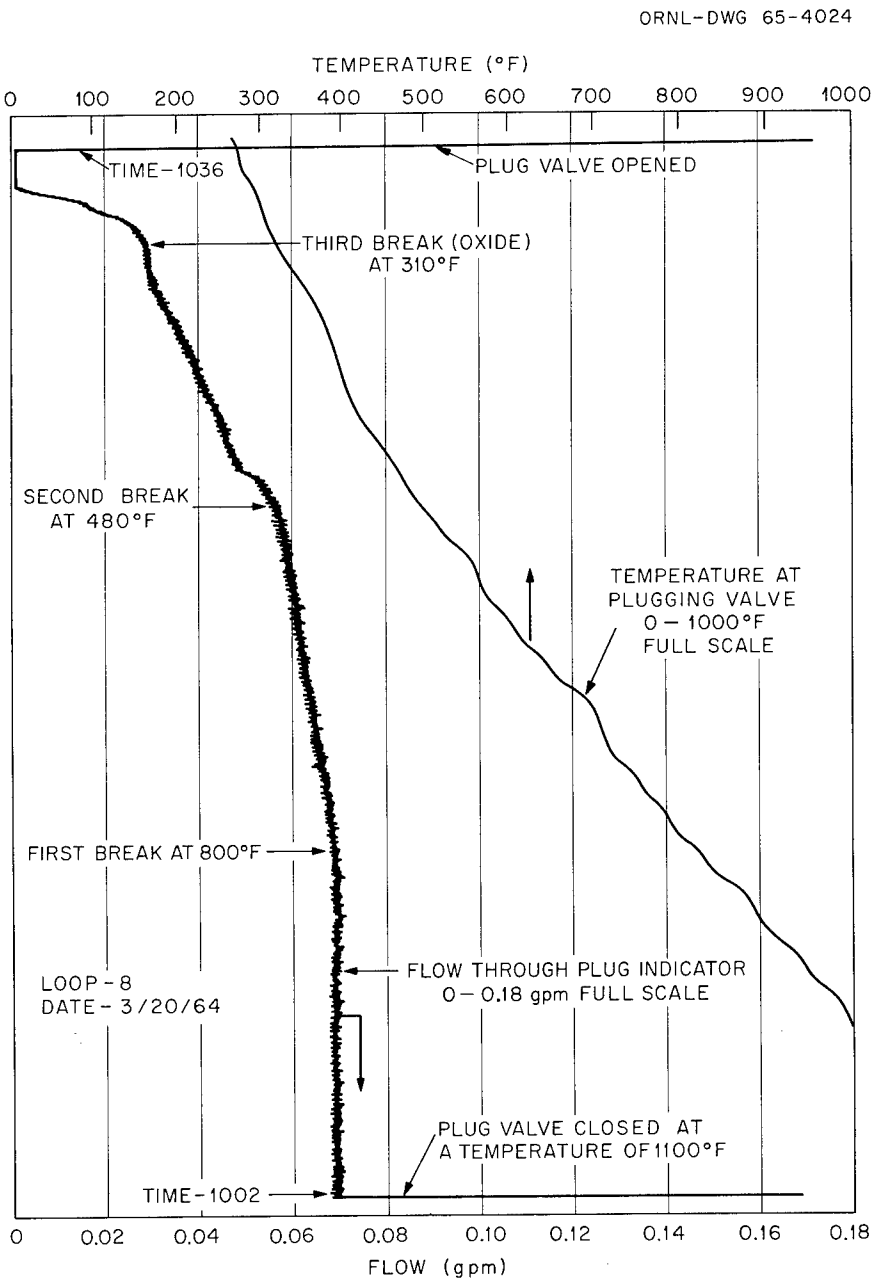

Fig. 2. Typical Three-Break Plugging Indicator Curve.

3. Hot trapping with zirconium foil at 1400°F has no effect on the initial break.

4. Injection of hydrogen at a rate of 0.6 cc (STP)/hr into five different loops has no effect on the characteristics of the plugging indicator curves.

5. Replacing the charge of NaK in the loop has no effect on the temperature at which the initial break occurs.

6. The temperature at which the initial break occurs usually decreases about 100°F during the first month of operation. Loop 5-5 was an exception in that the initial break point decreased 450°F during the first month.

7. The rate of flow decrease with a constant cooling rate is more gradual for the initial break than for subsequent breaks.

As mentioned in an earlier section of this report, an observable amount of argon was being transferred throughout loop 14-4 by differential temperature solubility in the NaK. A series of tests was therefore run on the loop 14-4 plugging indicator to demonstrate that argon coming out of solution during cooling was the cause of the initial break in flow. For these tests the NaK flow path was normal (see Fig. 1). The bypass stream passed through the economizer, through a cooler, and into the plugging valve, where it flowed through four small orifices in the plug-seat combination. By the use of external heaters, the tendency of the economizer to cool the incoming stream could be controlled, and the temperature at the inlet of the plugging indicator cooler could be adjusted as desired.

Three runs were made with inlet temperatures to the cooler of 1000, 800, and 625°F. Care was taken that temperatures significantly lower than these did not exist upstream. When cooling air was started through the precooler, initial breaks occurred at 800, 600, and 325°F, respectively. The fact that the initial break would consistently occur 200 to 300°F below the inlet temperature is believed to demonstrate that argon coming out of solution in the NaK as it passes through the cooler is the cause of the initial break. In addition, the presence of argon seems consistent with earlier observations made about the initial break. It is obvious that argon must also be coming out of solution as a result of any required cooling process upstream of the cooler; however, argon released at the economizer is trapped in the low-velocity downcomer that leads to the plugging indicator. Prolonged operation has shown that the vertical downcomer eventually fills with argon, and bubbles are then released in bursts.

Previous operation of loop 5-5 had shown that the temperature level of the initial break changed with accumulated operating time to a much greater degree than in the other loops. Postrun examination of five plugging indicator valves showed that a marked degree of erosion had occurred at the type 316 stainless steel valve seat of the loop 5-5 unit as compared with the others. This change in orifice configuration is believed to be the reason for the difference in the observed characteristic of the initial break.

Plugging runs were attempted on loop 14-4 with different argon cover gas pressures in the surge tank in an attempt to affect the behavior of the initial break and to further demonstrate that argon was a factor. This series of tests proved inconclusive because the argon pressure required to suppress boiling in the loop was apparently adequate to cause the plugging indicator initial break. No change in the initial break temperature was observed with the argon cover pressure maintained at levels of 8.8, 14.1, 19.7, and 24.7 psia. The loop could not be operated under a complete vacuum at the surge tank without modifications, which are presently not feasible.

The cause of the second break (400 to 600°F) phenomenon in the plugging indicator is unknown. Some observations on the second break are that:

1. The material responsible does not form as tenacious a plug as oxide and sometimes sweeps partially away.

2. Reheating runs made after partial plugging occurred showed that the material flushed away at about the same temperature that precipitation occurred.

3. This second plugging break is affected moderately by cold trapping, but is not as readily affected as the oxide break.

4. The rate of plugging from the second break is more gradual than from oxide precipitation.

5. Hot trapping at 1400°F with zirconium foil on loops 1A and 8 did not remove the second break, although the break temperature was reduced to the 410 to 460°F range.

6. The second break consistently became more pronounced in all low-oxide-content loops when either the hot traps or cold traps were isolated from service for two or more days.

7. Postrun examination of low-oxide-content loops (<30 ppm) 1A, 5, 8, 10, and 13 showed low corrosion rates of the 300 series stainless steels, as compared with high-oxide-content loops 2, 7, and 9. All the above-listed low-oxide-content loops had pronounced second breaks in the 400 to 600°F range. The corrosion results imply that the second break is caused by a material other than oxide.

CORROSION-LOOP MATERIAL STUDIES

A. Taboada B. Fleischer

Decarburization of Croloy 9M

As described previously,[11] fully annealed Croloy 9M sheet was decarburized down to 0.002 to 0.010% C in a type 316 stainless steel isothermal NaK loop at 1425°F. Tensile tests performed on this material and control material given the same thermal history revealed a significant reduction in the tensile strength at room temperature and at elevated temperature. The results of these tests are reported in Table 3.

Additional tests are in progress to determine the effect of decarburization on strain rate and creep-rupture life. A test program has also been planned for determining the effect of decarburization on the mechanical properties of standard Croloy 9M and modified Croloy 9M in the normalized temper-annealed condition. Two different normalizing temperatures will be used for each material.

---

[11]A. Taboada and B. Fleischer, Corrosion-Loop Material Studies, pp. 21–23, SNAP-8 Corrosion Program Quart. Progr. Rept. Nov. 30, 1964, USAEC Report ORNL-3784, Oak Ridge National Laboratory.

Table 3. Effect of Decarburization on Tensile Strength of Croloy 9M[a]

Temperature (°F)	Ultimate Strength (psi)		0.2% Yield Strength (psi)		Carbon Content of Decarburized Specimen (%)
	Control[b]	Decarburized	Control	Decarburized	
	× 10^3	× 10^3	× 10^3	× 10^3	
78	71.20	55.11	45.33	35.48	0.008
500	64.90	48.95	36.65	24.54	0.007
1100	27.6	22.0	19.07	16.33	0.005
1300	10.20	8.13	9.59	7.8	0.004
1400	6.08	4.32	5.81	3.92	0.004

[a]Control specimens were given same thermal history as decarburized specimens; fully annealed and heated 600 hr at 1425°F.

[b]Carbon content of control material was 0.12%.

Phase Identification Studies

Metallographic examinations of the types 347 and 316 stainless steel insert specimens exposed 2000 hr at 1300°F or higher in all the loops have revealed the presence of several metallurgical phases not originally present in the as-received microstructures. Consequently, some effort has been made to identify the new structures. The exposure temperature of 1300°F and the exposure period of 2000 hr are capable of causing precipitation of such phases as sigma, chi, and metal carbides, with their occurrence being dependent upon the existing chemical balance in the alloy. Several identification methods have been tried, such as the use of dilute and concentrated solutions of Murakami's reagents, as described by Emmanuel.[12] These reagents indicate the presence of both carbide and sigma-phase structures in types 347 and 316 stainless steel. In the type 347 stainless steel specimens (see Fig. 3) the phase indicated as carbides occurred in the portion of the specimen nearest to the surface that had been exposed to NaK, and the phase indicated as sigma occurred in the

[12]G. M. Emmanuel, Metal Progr., 53: 78–79 (1947).

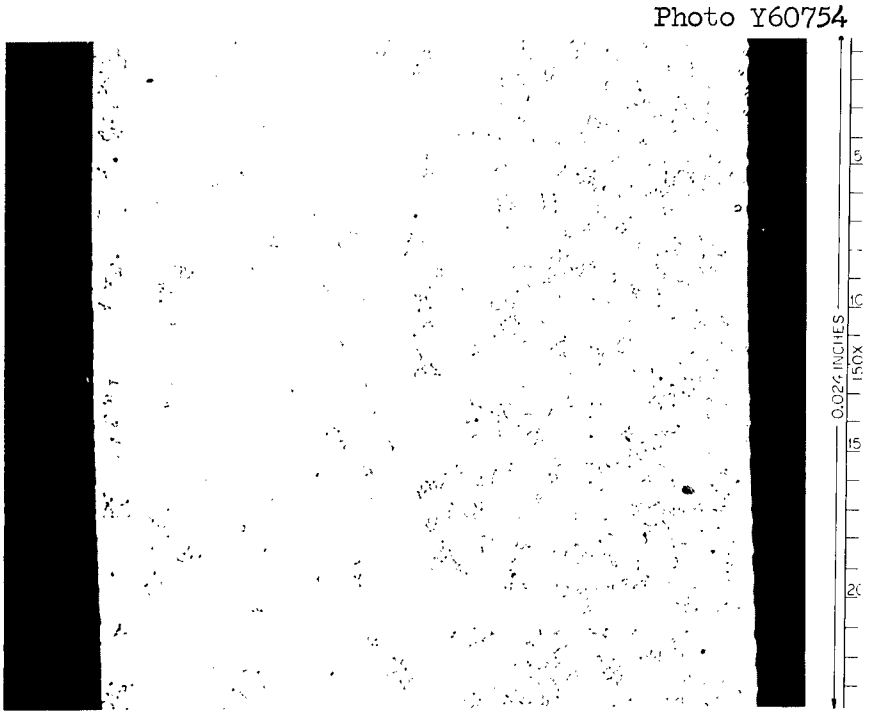

Fig. 3. Carbides (Dark Particles) and Sigma Phase (Light-Gray Particles) in Type 347 Stainless Steel Exposed to NaK at 1400°F for 5133 hr. Specimen No. 5, loop 5-5. Surface exposed to NaK is at right side of photograph.

other portion. Since the specimens were undergoing carburization through the surface exposed to NaK, the apparent separation of phases indicates that carbon enrichment was causing decomposition of sigma-phase material. This is consistent with the general theory regarding the sigma phase in austenitic stainless steels. The carbon acts as an austenite stabilizer. It also removes the chromium from the matrix by formation of chromium carbides, and thus it affects the matrix composition in favor of sigma-phase decomposition.

Identification of the phases present in type 347 stainless steel was also accomplished by extraction with an electrolytic solution of $FeCl_3$, as described by Barnett.[13] A sample of metal was dissolved, and the particulate phases were collected by centrifuge separation. X-ray diffraction analysis of the undissolved phases showed the presence of austenite,

[13]W. J. Barnett, Metal Progr., 53: 366–367 (1948).

Cr_7C_3, $(Fe,Cr)_{23}C_6$, and sigma phase. Similar analysis of type 316 stainless steel failed to reveal the presence of sigma phase, but it did show both carbides. There was also a weak unknown structure apparent in both alloys.

Identification of Mass Transfer Products

Chemical analysis of mass transfer deposits found in the various loop tests has demonstrated the presence of such elements as Cr, Ni, Mn, Fe, Mo, Na, and C. These have occurred as carbides and various alloys. In addition, metallographic evidence of an oxide mass transfer product was noted in the high-oxygen-content loops (see Fig. 4). X-ray diffraction analysis revealed a compound of the type NMO_2, where N is Na or K and M is Cr, Ni, or Fe. The complex oxide could be partially separated from magnetic mass-transfer products by vigorous agitation in water followed by extraction of magnetic materials. Electron microprobe analysis of deposits in situ clearly revealed that the complex was very high in

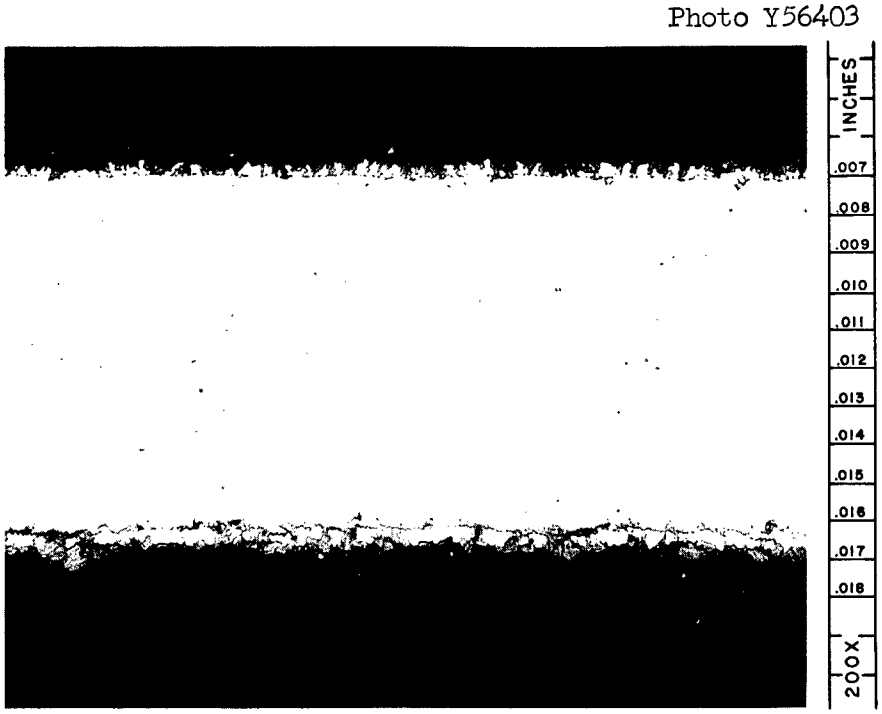

Fig. 4. Mass Transfer Products in Loop 9-2, Specimen No. 1. Surface deposits consist of metal particles (bright) and $NaCrO_2$ (gray).

chromium and contained no iron or nickel. Wet chemical analysis revealed the presence of sodium and thus indicated that the complex oxide is sodium chromite, $NaCrO_2$.

Status of Analytical Examinations of Corrosion Loops

The status of the analytical examinations is reported in Table 4 for the loop tests that have been completed. In general, the examinations show that very little metal migration occurs in low-oxygen-content NaK at temperatures up to an including 1400°F; however, carbon migration is quite severe. Corrosion of Croloy 9M in low-oxygen-content NaK is undetectable and that of types 347 and 316 stainless steel is very low, as compared with the corrosion of chromized Hastelloy N, which ranges from three to seven times greater. The oxygen level of the NaK is an important variable governing the corrosion rates of all the materials. At 1400°F, increasing the oxygen content of the NaK to approximately 80 ppm results in a low corrosion rate for Croloy 9M and causes the corrosion rate of types 347 and 316 stainless steel to increase by a factor of 3 to 4 over that experienced at the low oxygen level. However, the effect of this level of oxygen on the corrosion rate of Hastelloy N is very small.

Additions of hydrogen to the NaK have not produced any discernable effects on the mass transfer rate of any of the materials. Furthermore,

Table 4. Status of Loop Examinations

	Loop No.[a]									
	1-1	10-1	9-2	8-4	7-3	1A-1	2-2	4-4	5-5	13-3
Loop cutup and visual inspection	C	C	C	C	C	C	C	C	C	C
Posttest weighing of specimens	C	C	C	C	C	C	C	C	C	C
Carbon analysis of specimens	C	C	C	C	C	C	C	C	C	C
Carbon analysis of loop piping	C	C	C	C	C	C	C	C		
Metallographic examinations	C	C	C	C	C	C	C	C	C	I
X-ray fluorescence analysis	C	C	C	C	C				C	
Electron microprobe analysis		C	C							

[a]C indicates completed examinations; I indicates examinations in progress.

in the evaluations made to date, the extent of carbon migration does not appear to be significantly affected by the level of hydrogen or oxygen in the NaK within the concentration ranges being studied.

Phase identification studies performed on types 347 and 316 stainless steel specimens exposed in the loops have indicated that the loop exposures cause development of carbide phases and sigma phase. Results also indicate that in type 347 stainless steel the sigma phase gradually decomposes as carburization proceeds across the specimen.

Results of hot-spot loop test 13-3 showed less corrosion damage under conditions of very low NaK flow at the 1450°F hot spot temperature than under conditions of high velocity and a temperature of 1300°F. Examination of loop 5-5 showed both general and intergranular corrosion of Chromized Hastelloy N after 5133 hr at 1400°F.

Loop 4-4

Loop 4-4 operated 2000 hr with a maximum hot-leg temperature of 1425°F, a low oxygen content, and continuous hydrogen addition. Results of previous examination of this loop have been reported.[14] Recent examinations revealed the degree of decarburization of the Croloy 9M as determined by carbon profile studies. The hot upstream end exhibited a low-carbon (~0.002% C) ferrite field about 0.060 in. deep. About 2 ft downstream there was approximately one-half as much decarburization.

Loop 5-5

Loop 5-5 operated 5133 hr with a maximum hot-leg temperature of 1425°F, a low oxygen concentration, and continuous hydrogen addition. Posttest examination of the loop piping and specimens revealed very little mass transfer. The only visible evidence of corrosion-product buildup was a small amount of deposit on specimens in the vicinity of the electromagnetic pump. Weight-change data revealed a weight loss of about 19.8 mg/cm^2 for Hastelloy N at the hot end (~1400°F) of the heater section. Corrosion damage of Hastelloy N involved both general corrosion and intergranular attack, as shown in Fig. 5. General corrosion appeared

[14] Op. cit., ref. 11, pp. 32–33.

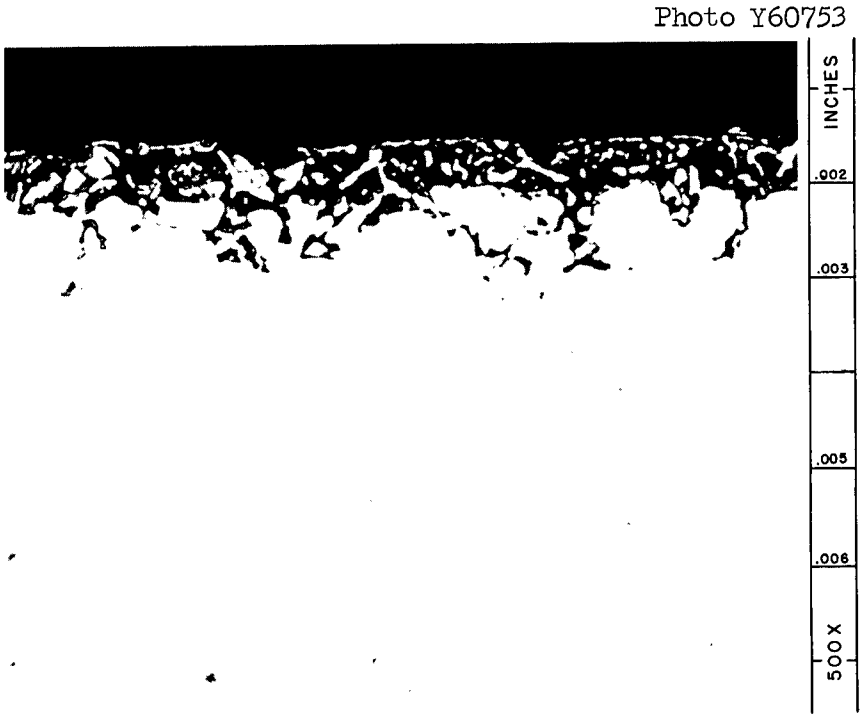

Fig. 5. General and Intergranular Corrosion of Hastelloy N Exposed in NaK at 1400°F for 5133 hr. Specimen No. 4, loop 5-5.

to be about 0.5 mil deep, whereas intergranular attack extended about 1 mil beyond the depth of general corrosion. No metallographic evidence of corrosion was found in any of the other materials; however, weight change data showed that the corrosion of type 347 stainless steel at the same temperature was about one-tenth that of Hastelloy N, and type 316 stainless steel located in a lower NaK velocity region was corroded about one-sixth as much as the type 347 stainless steel. The lower NaK velocity is believed to be responsible for the difference in the corrosion rates of these two basically similar materials. Within experimental error, Croloy 9M at 1385°F showed no corrosion. However, considerable carbon migration occurred, as determined by both carbon analysis of insert specimens and metallographic examination. At the hot upstream end of the Croloy 9M piping, the material was decarburized completely across the wall, as depicted in Fig. 6. Two feet downstream at the same temperature, decarburization had proceeded about three-fourths of the way

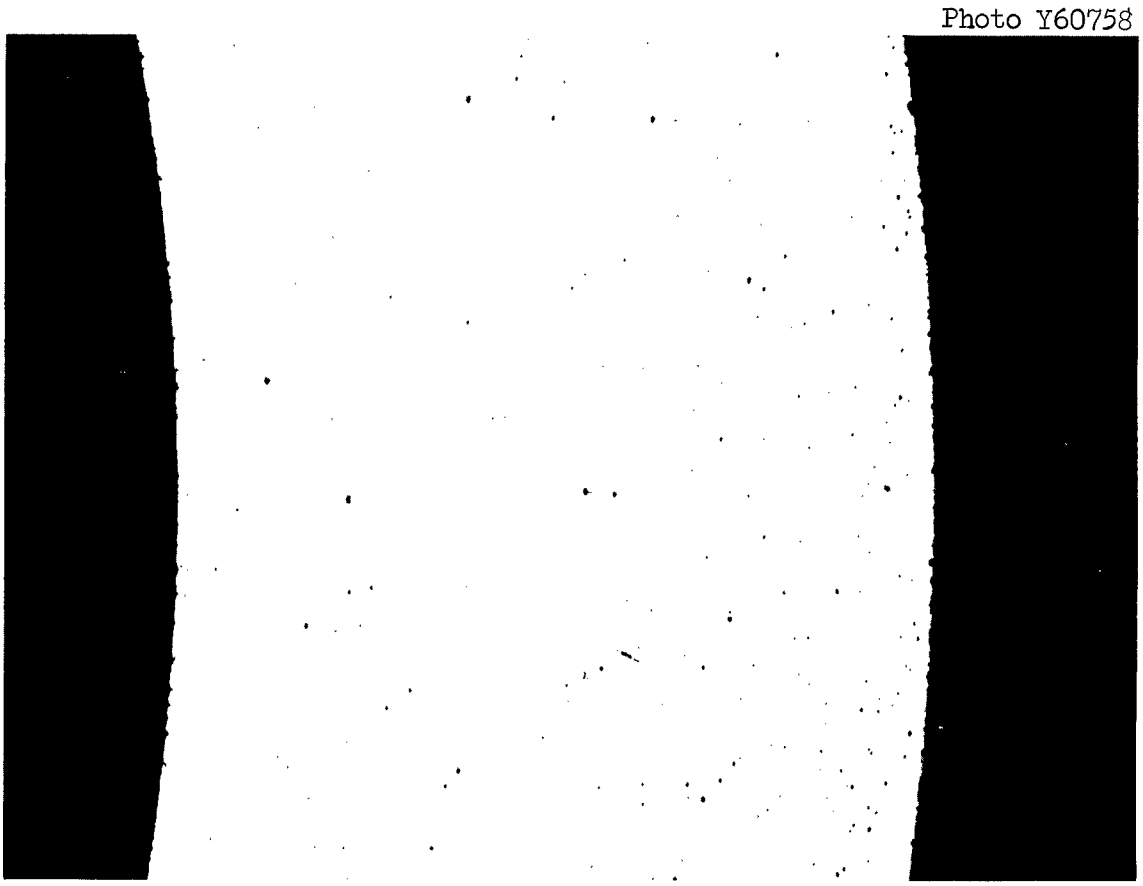

Fig. 6. Complete Decarburization Across Wall of 1-in.-OD, 0.122-in.-Wall Croloy 9M Tubing Exposed to NaK at 1385°F for 5133 hr. 39X

across the wall, as shown in Fig. 7. Both figures also reveal the extensive grain growth that accompanied decarburization. The general pattern of carbon migration around the loop was similar to that noted in all previous loops; however, the longer exposure time resulted in a greater degree of carbon migration. The carbon content of type 316 stainless steel at the hot end of the heat exchanger increased from about 0.054% to approximately 0.44%. Metallographic evidence of carburization is shown in Fig. 8. At the cold end of the heat exchanger, Croloy 9M was also carburized as indicated by the pre- and posttest carbon contents of specimens 8 and 9 (see Fig. 9 for specimen location diagram), which increased from about 0.11% to about 0.2%. Metallographic examination did not reveal this, as noted by the relative uniformity of carbides visible

Photo Y60759

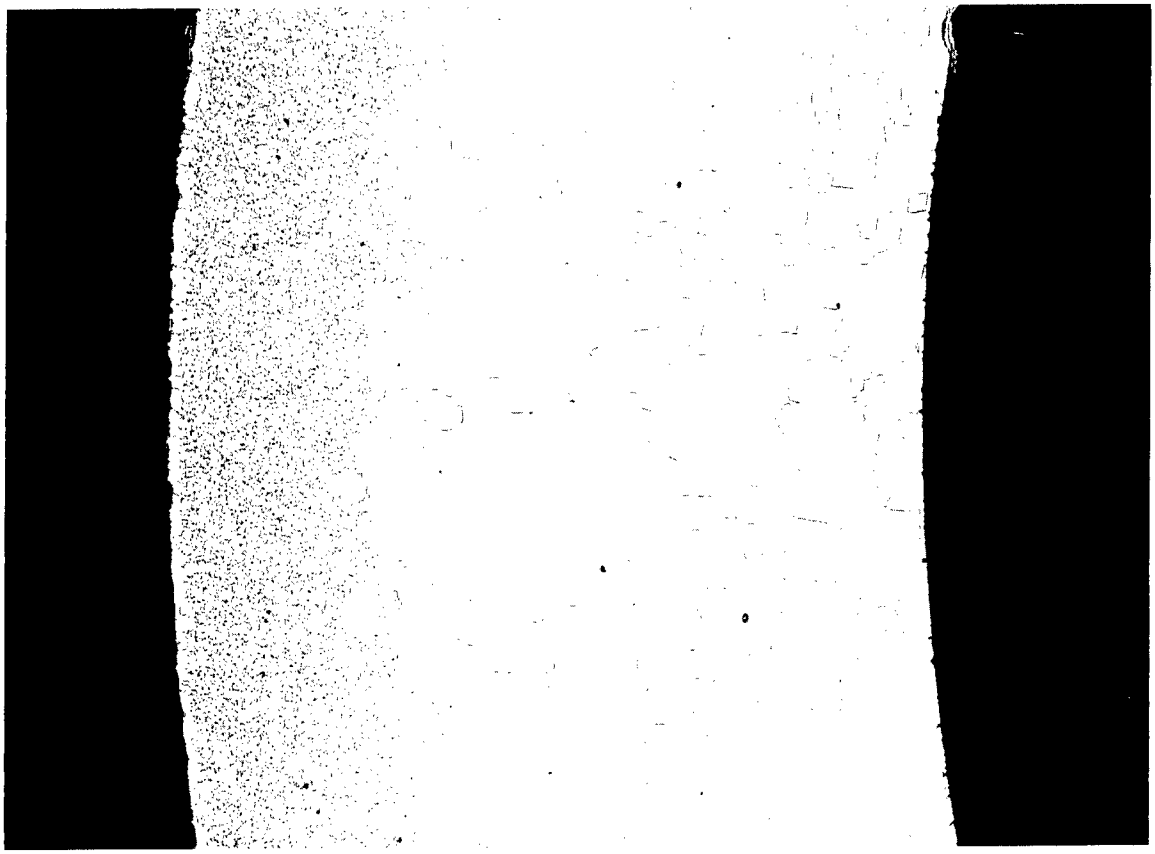

Fig. 7. Decarburized Croloy 9M Piping 2 ft Downstream of that Shown in Fig. 6. Same exposure conditions. 39X

in the cross section of specimen 8, shown in Fig. 10. The photomicrographs of Figs. 11 and 12, however, show clearly the difference in the carbide content of specimen No. 9, which was carburized to about 0.2% C, and specimen No. 10, which was decarburized to about 0.03% C. These two pictures also reveal the nickel-rich diffusion layer that resulted from dissimilar metal mass transfer. In the hot-leg portion of the loop, the carbon content of Hastelloy N specimen No. 4 increased from about 0.028 to 0.15%. All carbon contents quoted represent the average for a sample taken across the total thickness of the specimen.

Spectrographic analysis of mass transferred corrosion products deposited at the upper end of specimen 13 (Fig. 13) revealed the presence of approximately equal portions of Cr, Ni, and Mn. X-ray diffraction

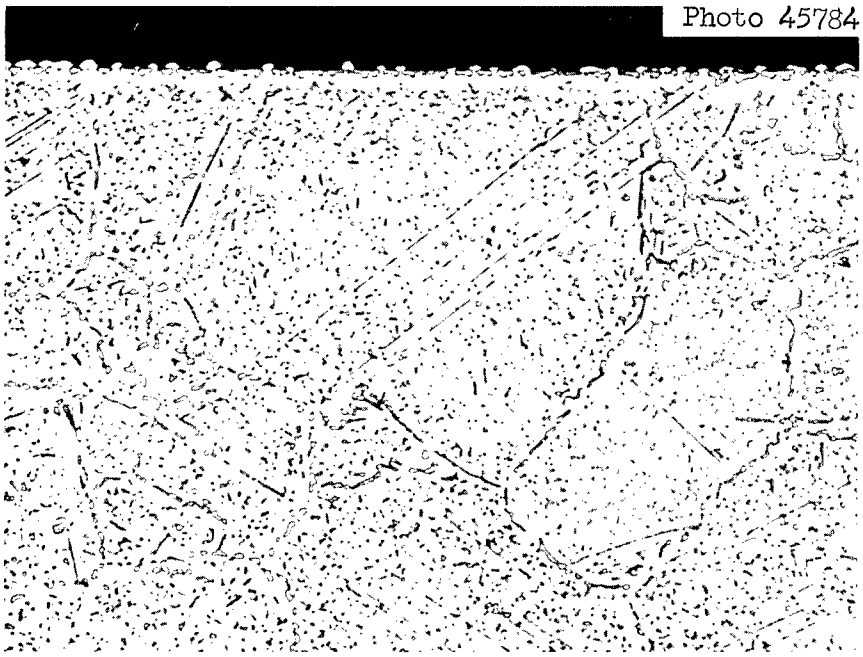

Fig. 8. Carburized Type 316 Stainless Steel Exposed to NaK at 1283°F for 5133 hr. Specimen No. 16, loop 5-5. 500X.

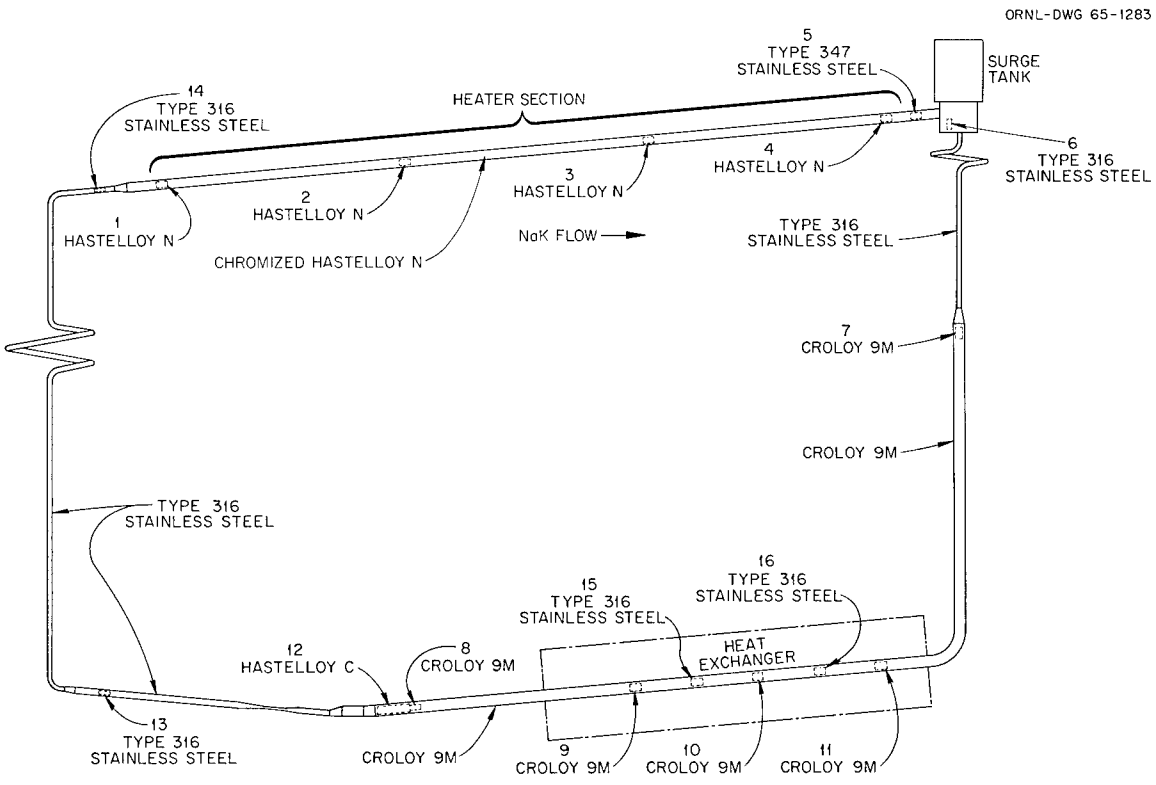

Fig. 9. Loop Design Showing Locations of Insert Specimens.

Photo Y60755

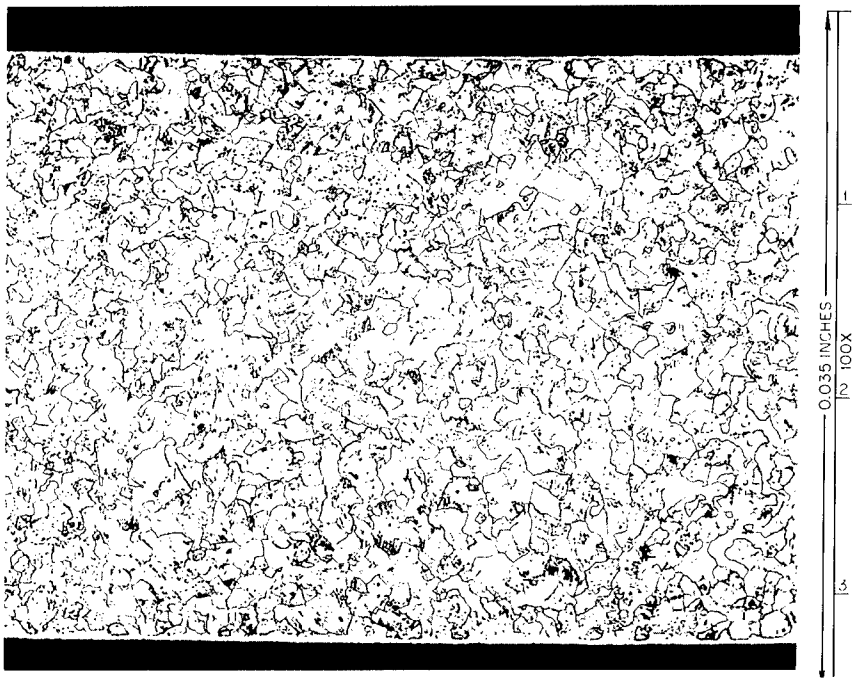

Fig. 10. Carburized Croloy 9M Exposed to NaK at 1110°F for 5133 hr. Specimen No. 8, loop 5-5.

Photo Y60756

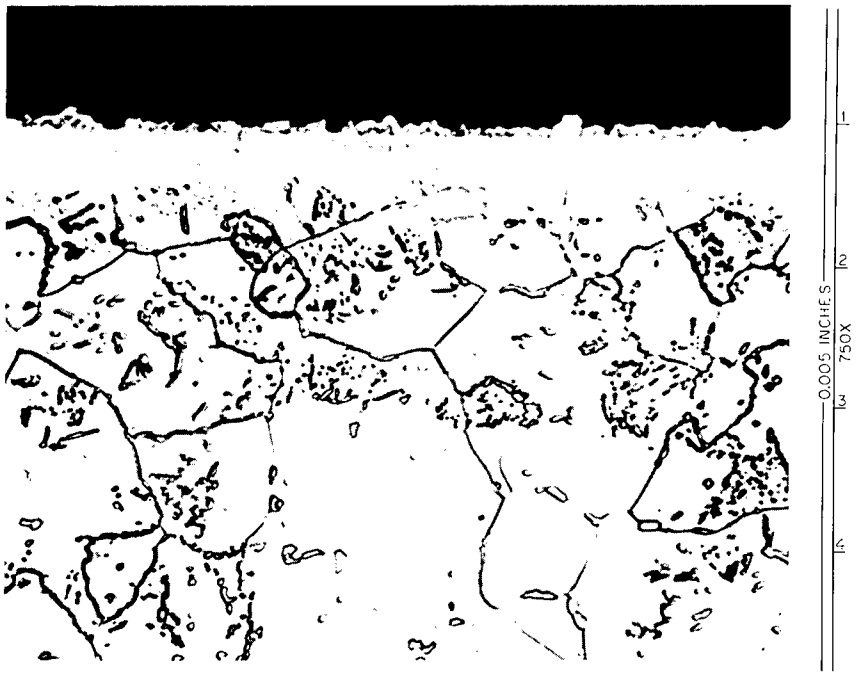

Fig. 11. Carburized Croloy 9M Exposed to NaK at 1160°F for 5133 hr. Specimen No. 9, loop 5-5.

Photo Y60757

Fig. 3.12. Decarburized Croloy 9M Exposed to NaK at 1242°F for 5133 hr. Specimen No. 10, loop 5-5.

Photo 71814

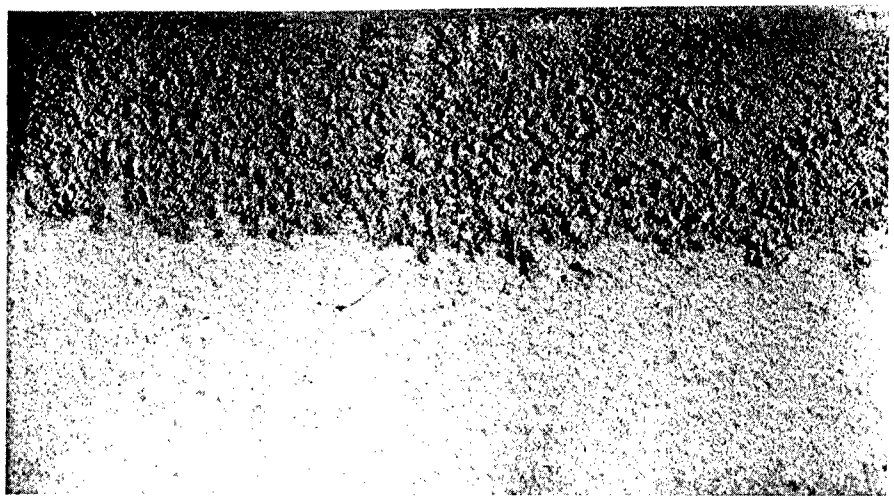

Fig. 13. Mass Transfer Products at Upstream End of Specimen No. 13. Loop 5-5. ~9X

analysis indicated that these elements were present both as solid-solution alloys and carbides. The principal constituent was a face-centered-cubic structure tentatively identifiable as γNi-Mn possessing approximately 15 at. % Mn.

Loop 13-3

Loop 13-3 operated for a total of 2000 hr with the main loop maximum hot-leg temperature at 1300°F and a bypass hot-spot section heated to 1450°F. The oxygen was maintained at a low level, and hydrogen was continuously added. Posttest examination of the loop piping and specimens revealed no visible evidence of corrosion. Weight-change data showed very low corrosion rates for all the materials. The maximum corrosion occurred at the hot end (~1300°F) of the heater section, where Hastelloy N corroded about 2.2 mg/cm^2. Downstream at the same temperature, type 347 stainless steel corroded about one-half as much as Hastelloy N, and type 316 stainless steel in a lower NaK velocity region corroded about one-third as much as type 347 stainless steel. In the low-NaK-velocity hot-spot section, the Hastelloy N at 1450°F was corroded approximately 1.7 mg/cm^2.

Metallographic examination of the Croloy 9M revealed very slight decarburization approximately equivalent to that found in loop 8-4, which was also a 1300°F loop with continuous hydrogen addition. The extent of carbon migration in these two loops was considerably less than that experienced in the other 1300°F loops.

CHEMISTRY STUDIES

E. L. Compere H. C. Savage
J. E. Savolainen T. H. Mauney

Hydrogen Permeation Studies

Deuterium Permeation of Type 316 Stainless Steel

The planned injection of deuterium instead of hydrogen into loop 14-4, as mentioned in the preceding section on "Forced-Flow Corrosion-Loop Experiments," could relieve problems arising from traces of normal

hydrogen in the atmosphere and in the argon used as a sleeve sweep gas. It was desirable therefore to verify the anticipated drop in permeability, which was expected to be the square root of the atomic weight ratio, or $1/\sqrt{2}$. For the necessary measurements, hydrogen was replaced with deuterium in the existing type 316 stainless steel cell containing NaK, which was used to obtain the extensive hydrogen permeation data reported previously.[15] Performing the permeation measurements in the same cell provided for direct comparison of the hydrogen and deuterium results.

Deuterium permeation data were obtained at 1100 and 1300°F and at pressures of approximately 1 atm and 200 mm. The data are listed in Table 5, along with those of previous tests in the same cell with normal

Table 5. Permeation of Hydrogen and of Deuterium Through Type 316 Stainless Steel in the Presence of NaK at 1100 and 1300°F

Pressure (mm Hg)	Hydrogen Permeability [cc (STP) mm hr^{-1} cm^{-2} $atm^{-1/2}$]		Pressure (mm Hg)	Deuterium Permeability [cc (STP) mm hr^{-1} cm^{-2} $atm^{-1/2}$]	
	At 1100°F	At 1300°F		At 1100°F	At 1300°F
760		0.288	731	0.0908	
		0.294		0.0889	
206		0.297	213	0.0918	
204		0.292	203	0.0924	
747	0.132		178		0.210
	0.132				
			700		0.219
					0.224
216	0.135				
	0.134				
Average	0.133	0.293		0.0910	0.218

hydrogen at comparable temperatures and pressures. The deuterium results, which are listed in the sequence in which the measurements were made, were obtained after carefully evacuating both sides of the permeation cell for one day. The leak rate of the system at temperature was 1 μ/hr on the upstream side and less than that on the downstream side before

[15] E. L. Compere and J. E. Savolainen et al., Chemistry Studies, pp. 53–57, SNAP-8 Corrosion Program Quart. Progr. Rept. Nov. 30, 1964, USAEC Report ORNL-3784, Oak Ridge National Laboratory.

deuterium was added to the system. Mass spectrometric analysis of the feed gas showed 99.95% D_2, and only one permeated gas sample was slightly less than 99.0% deuterium.

The ratio of permeabilities of deuterium and hydrogen was 0.68 at 1100°F and 0.74 at 1300°F. These values compare satisfactorily with the anticipated ratio of 0.71.

Hydrogen Permeation After Oxidation of Stainless Steel

Subsequent to the deuterium tests, the stainless steel cell was purged of deuterium, and tests with hydrogen were continued. Studies were made of the effects on hydrogen permeation of air oxidation of the downstream surface of the type 316 stainless steel diaphragm. Prior to oxidation the system was operated at temperature in order to attain steady-state hydrogen permeation in the cell. The feed gas contained 99.91 mole % hydrogen. Permeation coefficients were determined for comparison with those reported in the previous section (Table 5) and for comparison with values to be obtained after oxidation. The hydrogen permeation coefficient of the diaphragm at various pressures was independent of pressure, as shown in the first part of Table 6 (see experiment No. 8). The values ranged from 0.114 to 0.129 cc (STP) mm hr^{-1} cm^{-2} $atm^{-1/2}$, in fair agreement with the value of 0.133 from Table 5.

First Oxidation Experiment (1100°F). Before admitting air to the downstream chamber of the cell, hydrogen was supplied at a pressure of 1 atm to the upstream side of the cell, and permeation was continued for 23 hr with a downstream vacuum to establish a steady state. Ambient air (at 1-atm pressure) was then admitted to the downstream chamber for 10 min. In this experiment, the downstream side was then evacuated for 15 min, and the gases were discarded. Collection and measurement of the permeating gas by means of the Toepler pump were then resumed. Data from this experiment are tabulated in Table 6 (see experiment No. 1). Collection of gas over four periods totaling 28.6 hr, with the first three gas samples being analyzed, showed that the earlier samples contained a substantial proportion of water, which decreased in subsequent samples. This is presumed to be the product of reaction between permeating hydrogen and metal oxide.

Table 6. Effect of Air Oxidation on Permeation of Hydrogen Through a Type 316 Stainless Steel Diaphragm

Experiment No.	Conditions	Post-oxidation Time (hr)	Pressure of Feed (mm)	Volume of Gas Collected [cc (STP)]	Sample Collection Time (hr)	Permeation Rate [cc (STP)/hr]	Hydrogen Permeation Coefficient[a]	Analysis (mole %)				
								H_2	H_2O	CO_2	O_2	N_2
0	Preoxidation determination at 1100°F	0	733				0.124					
			731				0.122					
			224				0.129					
			224				0.125					
			55				0.114					
			49				0.128					
1	Downstream chamber at 1100°F; exposed to air for 10 min and evacuated for 15 min	4.3	742	0.163	4.0	0.040	0.047	83.97	14.18	0.55	0.01	1.24
		6.8	742	0.193	2.0	0.096	0.116	97.54	1.80	0.08	0.02	0.40
		26.0	733	0.198	2.0	0.099	0.121	99.52	0.05	0.04	0.01	0.34
		28.6	731	0.201	2.0	0.100	0.123	Not analyzed				
2	Downstream chamber at 1100°F; exposed to air for 10 min; air recovered											
	Air recovered by Toepler pump after 10 min oxidation	0.25	723	12.301	0.25			0.04	0.40	0.04	18.04	80.46
	Hydrogen collected	2.8	723	0.149	2.5	0.060	0.050	25.62	43.13	1.02	3.66	26.19
		4.8	721	0.193	2.0	0.096	0.117	63.02	35.21	0.35	0.04	1.33
		6.8	719	0.206	2.0	0.103	0.126	75.02	23.82	0.15	0.03	0.92
		71.8	682	7.047	65.0	0.108	0.136	96.80	2.56	0.04	0.01	0.47
3	Downstream chamber at 1300°F; exposed to air for 10 min; air recovered											
	Preoxidation determination		723	0.240	1.0	0.240	0.293	99.25	0.17	0.03	0.02	0.45
	Air recovered by Toepler pump after 8 min oxidation	0.2		11.934				0.10	0.39	0.04	1.67	96.55
	Hydrogen collected	1.9	717	0.294	1.75	0.168	0.197	42.72	52.21	1.51	0.16	3.26
		2.7	717	0.212	0.75	0.282	0.342	76.03	22.13	0.24	0.08	1.41
		3.2	717	0.130	0.50	0.261	0.317	14.96	14.96	0.15	0.08	1.40

[a] Permeation coefficient, cc (STP) mm hr^{-1} cm^{-2} $atm^{-1/2}$; both H_2 and H_2O are included in the calculation.

The permeation coefficient for the first period (4 hr) was less than 40% of the value before oxidation. However, as permeation continued, the permeation ceofficients approached the preoxidation values.

Second Oxidation Experiment (1100°F). After completion of a total of two days hydrogen permeation at 1100°F after the first oxidation, ambient air was again permitted to enter the downstream region of the permeation cell, where it remained for 10 min. In this experiment, the air was recovered by the Toepler pump. Collection and measurement of the permeating gas by means of the Toepler pump were continued for a period of almost 72 hr, with four samples being taken. Data from this experiment are also tabulated in Table 6 (see experiment No. 2). It may be observed from the data that the major portion of the atmospheric oxygen was recovered unreacted at 1100°F. However, appreciable portions (which diminished in successive samples) of the permeating hydrogen were found in the form of water. The permeation rate, less than 40% of the preoxidation value, increased in successive samples to equal preoxidation levels.

Third Oxidation Experiment (1300°F). After completion of about 72 hr of hydrogen permeation after the second oxidation, the temperature was increased to 1300°F, and hydrogen permeation was continued for approximately two days with 1-atm pressure upstream and a diffusion pump vacuum downstream. Permeating gas was then collected for a preoxidation determination of the permeation coefficient, which agreed with the values at this temperature given in Table 5.

Ambient air was permitted to enter and remain in the downstream chamber of the permeation cell for a period of 8 min, after which it was collected with the Toepler pump for measurement and analysis. Most of the oxygen was consumed in this sample. Collection of the permeating gases was continued for a period of 3 hr, and, three samples were obtained. The permeation coefficient for the earlier (1.75-hr) period was about 65% of the preoxidation value. The two subsequent determinations somewhat exceeded the preoxidation value. Substantial portions of the hydrogen were found in the form of water in these samples. Data for this experiment are presented in Table 6 (see experiment No. 3).

Discussion. During the second (1100°F) and third (1300°F) oxidation experiments the Toepler pump was halted at intervals to permit several volumetric measurements to be made before a sample was removed for analysis. The variation in gas collection rates thus found is depicted in Fig. 14. By appropriate selection of different scales for plotting the measurements at the respective temperatures, the rate charts for the two experiments are shown to be similar. It is of considerable interest to note that the achievement of a rate equaling that of an unoxidized diaphragm is, in each case, preceded by a short period of unusually high rate. One explanation of such a phenomenon would be that the final removal of a surface resistance to permeation acted to release hydrogen "pent up" behind the barrier layer and dissolved in the metal of the

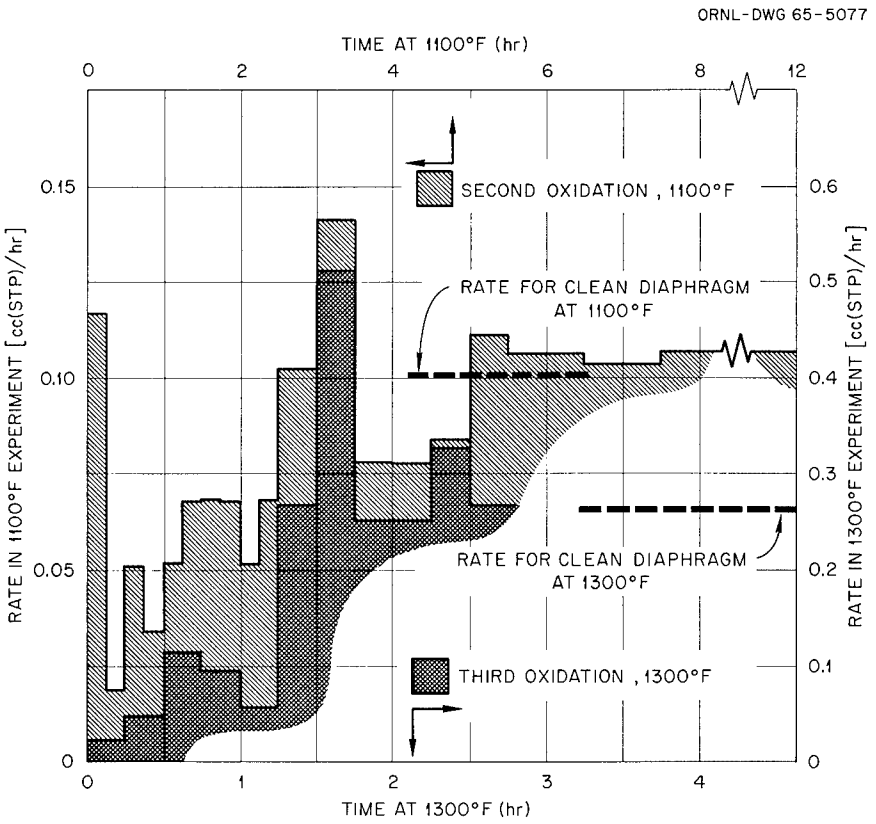

Fig. 14. Comparison of Hydrogen Permeation Rate Through Type 316 Stainless Steel Exposed to Air at 1100°F and at 1300°F on Adjusted Rate and Time Scales.

diaphragm. The variation of the observed permeation rate with time before the final steady rate is reached may be caused by stepwise removal by reduction of different oxide species as the hydrogen permeates to the surface. The study of the kinetics of these processes should serve to better determine the mechanism and could aid in devising more effective barriers to permeating hydrogen.

These experiments indicate that brief air oxidation of type 316 stainless steel results in an appreciable reduction of permeability. This persists, but it is removed by the passage of hydrogen. Studies of the effects accompanying more substantial oxidation are not funded.

Hydrogen Solubility Studies

Dissolution of Hydrogen Gas in NaK-78 and Precipitation of Solid Hydride

Data on the solubility of hydrogen in NaK-78 at 1300, 1100, 1000, 752, 626, and 572°F were reported previously[16] as a function of hydrogen pressures from a few mm up to 1 atm. There was evidence of the precipitation of a solid hydride in the determinations at the lower three temperatures.

The relationships between hydrogen pressure and the concentration of dissolved hydrogen, temperature, and the solubility of solid hydride are of appreciable interest in considering the fate of hydrogen in liquid alkali metals used for coolants in reactors, including SNAP-8. A diagram depicting these relationships and based entirely on our experimental observations is shown in Fig. 15. In this figure two coordinated charts are used, with the ordinate for each being the logarithm of the concentration of dissolved hydrogen (in ppm). In the left chart, this is plotted against the logarithm of hydrogen partial pressure in atmospheres. The slope of one half for the experimentally determined lines indicates agreement with Sievert's law for the solubility of gaseous hydrogen. The break upward in the lines for 572, 626, and 752°F indicates the precipitation of solid hydride. The position of the break locates the solubility of solid hydride and the decomposition pressure at this temperature.

---

[16]Ibid., pp. 48–53.

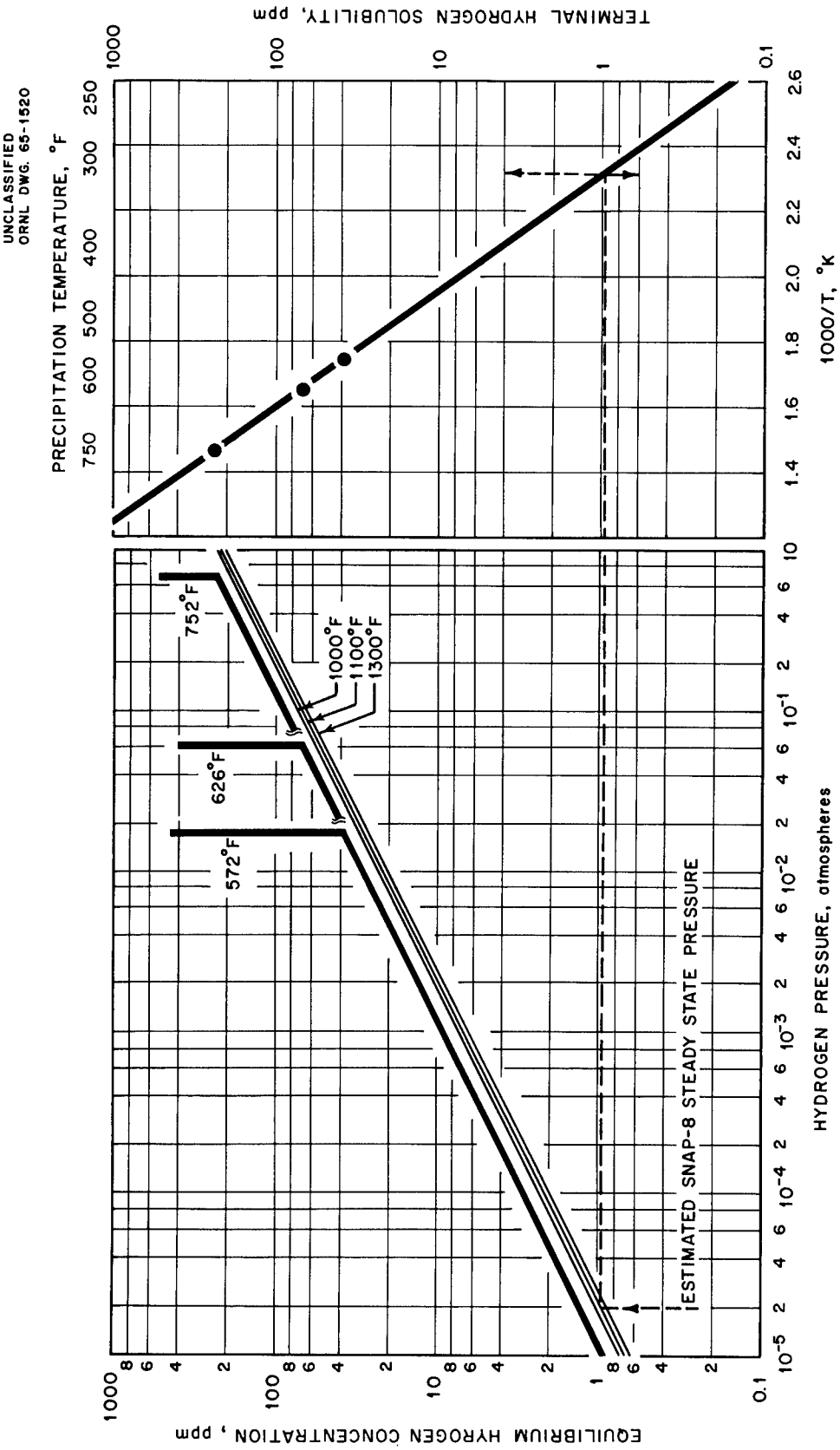

Fig. 15. Dissolution of Hydrogen Gas in NaK-78 and Precipitation of Solid Hydride.

In the right chart, these solid hydride solubilities are plotted as logarithms against the inverse of absolute temperature. A straight line results, as implied by theory. As an example of a use of the chart, the steady-state hydrogen pressure in the SNAP-8 primary coolant was estimated[17] to be 2.4×10^{-5} atm at 1100°F. Such a partial pressure should result in a hydrogen concentration in the NaK of about 1 ppm, as depicted by the dotted line on the diagram. This concentration of hydrogen in the NaK should result in precipitation of solid hydrides at temperatures slightly above 300°F. Any cold trapping to remove hydrogen from the coolant would have to be conducted below this temperature. If this solution were cooled in any region of the system to this temperature or below, solid hydride deposits should be anticipated there. The magnitude of such deposits would depend on various factors, including the interchange of NaK between this region and the rest of the system.

Phase Equilibria in the H–Li–NaK-78 System

Studies of the phase equilibria of the Na-K-Li-H system at 1100°F were reported previously.[18] This system is of interest because of the possibility of using a lithium addition to control the hydrogen activity in the SNAP-8 primary coolant by cold trapping at reasonable temperatures. In order to explore this possibility further, determinations have been made at 1000°F of the solubility of hydrogen in NaK-78 containing added lithium.

An Armco iron capsule containing 9.548 g of NaK-78 with 0.028 g added lithium (1.39 at. %) was placed in a quartz envelope. The amount of hydrogen taken up by the liquid metal at 1000°F was determined at various pressures between approximately 5 and 55 mm. Data from this experiment are listed in Table 7 in the order obtained.

These data, and data[18] from the experiments at 1100°F, are shown in Fig. 16, where the logarithm of the hydrogen absorption per gram of NaK-78

---

[17]E. L. Compere and J. E. Savolainen et al., Chemistry Studies, pp. 32–44, SNAP-8 Corrosion Program Quart. Progr. Rept. Aug. 31, 1964, USAEC Report ORNL-3730, Oak Ridge National Laboratory.

[18]Op. cit., ref. 15, pp. 35–48.

Table 7. Absorption of Hydrogen at 1000°F by NaK Containing 1.39 at. % Lithium

NaK-78: 9.54g
Li: 0.028 g

Pressure (mm Hg)	Hydrogen Absorbed [cc (STP)]	Measurement Made After Hydrogen Addition or Removal
9.1	5.75	Addition
6.6	5.23	Removal
5.3	4.62	Removal
5.0	4.08	Removal
7.9	8.04	Addition
10.3	11.93	Addition
10.2	11.92	Removal
21.6	22.03	Addition
21.0	22.01	Removal
54.8	31.92	Addition
53.8	32.00	Removal

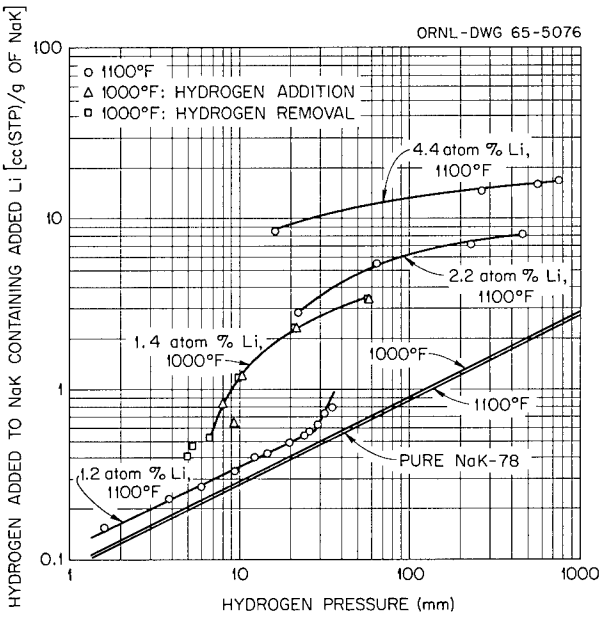

Fig. 16. Absorption of Hydrogen by NaK Containing Added Lithium.

is plotted against the logarithm of the pressure. Lines showing hydrogen solubility in pure NaK-78 are also given.

It is evident in all cases that the addition of lithium greatly lowered the partial pressure of hydrogen at an equivalent hydrogen addition. A hypothesis of a mechanism explaining this was previously described[18] in which the hydrogen combined with the respective alkali metals in proportion to their concentration and affinity for hydrogen. Limited solubility of the lithium hydride resulted in precipitation, which inhibited pressure change until the available lithium was exhausted. The solubility limit was indicated by an upward break (or "knee") from the Sievert's slope of one half.

Such a break was sought in the present experiment. A procedure was followed of adding enough hydrogen to exceed the anticipated Sievert's value, and subsequently obtaining equilibrium points after removing hydrogen until the data appeared to exhibit a Sievert's relationship. After this, larger quantities were to be added until an appreciable portion of the lithium was precipitated. This initial procedure was followed in order to avoid or relieve any permeation resistance due to development of oxide films on the outer surface of the iron capsule. Experiments previously reported[16] for pure NaK-78 had indicated the possibility of such resistances.

It appears that the establishment of equilibrium for the earliest points, the first four, is not certain, although they are included in the data. Consequently we have not attempted to use these points to find the break to the Sievert's region or to elaborate the data by the calculation of equilibrium constants, which require Sievert's region data.

At the conclusion of the hydrogen addition experiments, the hydrogen was recovered from the envelope, and the contents of the capsule were analyzed. The hydrogen material balance resulting from these measurements is given in Table 8.

As indicated above the data of this experiment clearly show a very substantial effect on hydrogen pressure resulting from the addition of lithium and the precipitation of lithium hydride.

Table 8. Hydrogen Material Balance in Hydrogen Addition Experiments

Experiment temperature	
°F	1000
°K	811
Terminal pressure, mm Hg	53.8
Weight of original loading, g	
NaK	9.548
Li	0.028
Weight of recovered loading, g	
NaK	9.33
Li	0.01696
Hydrogen inventory, cc (STP)	
Hydrogen measured into envelope	32.398
Accumulated permeation loss	0.131
Net hydrogen	32.267
Hydrogen recovered, cc (STP)	
Envelope dead space	0.185
Capsule vapor space	0.010
Analyzed in recovered NaK	14.8
Estimated from Li in insoluble residue	25.5
Total recovered	40.495
Net hydrogen inventory recovered, %	125

ORNL-3823

UC-33 – Propulsion Systems and
Energy Conversion
TID-4500 (41st ed.)

Internal Distribution

1. G. M. Adamson, Jr.
2. J. M. Baker
3. S. E. Beall
4. M. Bender
5. E. G. Bohlmann
6. D. W. Cardwell
7. C. E. Center (K-25)
8. E. L. Compere
9. F. L. Culler
10. J. H. DeVan
11. B. Fleischer
12. A. P. Fraas
13. W. R. Grimes
14. W. R. Huntley
15. W. H. Jordan
16. C. E. Larson (K-25)
17. H. G. MacPherson
18. R. E. MacPherson
19. A. J. Miller
20. H. C. Savage
21. H. W. Savage
22. A. W. Savolainen
23. J. E. Savolainen
24. M. J. Skinner
25. A. Taboada
26. A. M. Weinberg
27. J. C. White
28-29. Y-12 Document Reference Section
30-31. Central Research Library
32-36. Laboratory Records Department
37. Laboratory Records, LRD-RC

External Distribution

38. Aerojet-General Corporation, Sacramento
39. Aerojet-General Nucleonics (NASA)
40. Aerospace Corporation
41. Aerospace Test Wing (AFSC)
42. Air Force Surgeon General
43. Air University Library
44. Airesearch Mfg. Company, Phoenix
45. Army Ballistic Research Laboratory
46. Army Weapons Command
47. Aro, Inc.
48. Bendix Corporation (AF)
49-50. Canoga Park Area Office
51. Central Intelligence Agency
52. Department of the Army
53. Director of Defense Research and Engineering (OAP)
54. Douglas Aircraft Co., Inc., Newport Beach
55. Electro-Optical Systems, Inc.
56. Foreign Technology Division (AFSC)
57. General Dynamics/Astronautics (AF)
58-59. General Electric Company (FPD)
60. General Electric Company (MSVD)
61. Martin-Marietta Corp., Denver

62. Monsanto Dayton Laboratory
63-64. NASA Goddard Space Flight Center
65. NASA Marshall Space Flight Center
66. Naval Air Development Center
67. Naval Underwater Ordnance Station
68. Naval Marine Engineering Laboratory
69-70. Office of the Chief of Naval Operations (OP-03EG)
71. Office of the Chief of Transportation
72. Pratt and Whitney Aircraft Division (NASA)
73. School of Aerospace Medicine
74. USAF Headquarters
75. Westinghouse Electric Corp., Lima
76. Westinghouse Electric Corp., Lima (AF)
77. Division of Research and Development, AEC, ORO
78-79. Reactor Division, AEC, ORO
80-651. Given distribution as shown in TID-4500 (41st ed.) under Propulsion Systems and Energy Conversion Category (75 copies - CFSTI)

NASA Distribution Order No. C-220-A

652-654. NASA, Washington, D.C.
Att: P. R. Miller (RNP), F. Schulman (RNP), George C. Deutsch (RR)
655-656. NASA Scientific and Technical Information Facility, Bethesda, Maryland, Att: NASA Representative
657. NASA Ames Research Center, Moffet Field, California
Att: Librarian
658. NASA Goddard Space Flight Center
Att: Librarian
659. NASA Langley Research Center
Att: Librarian
660. NASA Manned Spacecraft Center
Att: Librarian
661. NASA George C. Marshall Space Flight Center
Att: Librarian
662. NASA Jet Propulsion Laboratory
Att: Librarian
663-678. NASA Lewis Research Center
Att: Librarian (2 copies), Henry O. Slone, Bernard Lubarsky, D. G. Beremand, P. L. Stone (2 copies), J. P. Merutka, R. W. Schaupp, L. E. Light, Norman T. Musial, Reliability and Quality Assurance Office, T. A. Moss, Louis Rosenblum, R. F. Mather, I. I. Pinkel
679. NASA Western Operations Office, Santa Monica, California
Att: John Keeler
680-681. NASA Western Operations Office, Azusa Field Office
Att: J. G. Kennard, F. Herrmann
682-685. Aeronautical Systems Division, Wright-Patterson Air Force Base
Att: George E. Thompson, Librarian, George Sherman, T. Cooper

686-687. U.S. Atomic Energy Commission, Washington, Technical Reports Library, Att: J. M. O'Leary
688. U.S. Atomic Energy Commission, CANEL Project Office
Att: Herbert Pennington
689-690. U.S. Atomic Energy Commission, Germantown
Att: Col. E. L. Douthett, Herbert Rochen
691-692. U.S. Atomic Energy Commission, Technical Information Service Extension
693-694. U.S. Atomic Energy Commission, Washington
Att: M. J. Whitman, J. D. Lafleur
695. Argonne National Laboratory
Att: Librarian
696-698. Brookhaven National Laboratory
Att: Librarian, D. Gurinsky, C. Klamut
699-701. Thompson Ramo Wooldridge, Inc.
Att: Librarian, E. Vargo, E. E. Steigerwald
702. U.S. Naval Research Laboratory
Att: Librarian
703. Advanced Technology Laboratories
Att: Librarian
704-706. Aerojet-General Corporation
Att: Librarian, R. S. Carey, H. Derow
707-710. Aerojet-General Nucleonics
Att: Librarian, B. Farwell, P. Young, M. Parkman
711-713 AiResearch Manufacturing Company, Phoenix
Att: Librarian, E. A. Kovacevich, John Dannen
714. AiResearch Manufacturing Company, Los Alamos
Att: Librarian
715-718. Atomics International
Att: Librarian, John Page, H. Gereke, Carl E. Johnson
719. AVCO, Research and Advanced Development Department
Att: Librarian
720. Babcock and Wilcox Company, Alliance, Ohio
Att: Librarian
721. Battelle Memorial Institute
Att: Librarian
722. The Boeing Company
Att: Librarian
723. Curtiss-Wright Corporation
Att: Librarian
724. E. I. DuPont de Nemours and Company, Inc.
Att: Librarian
725. Electro-Optical Systems, Incorporated
Att: Librarian
726. Ford Motor Company, Aeronutronics
Att: Librarian
727. General Atomic, John Jay Hopkins Laboratory
Att: Librarian
728. General Electric Company, San Jose
729. General Electric Company, Vallecitos
Att: Librarian

730. General Motors Corporation, Allison Division
Att: Librarian
731. Hamilton Standard
Att: Librarian
732. Hughes Aircraft Company
Att: Librarian
733-734. Lockheed Missiles and Space Division
Att: Librarian, John N. Cox
735. Marquardt Aircraft Company
Att: Librarian
736. The Martin Company
Att: Librarian
737. The Martin Company, Nuclear Division
Att: Librarian
738. Martin-Marietta Corporation, Metals Technology Laboratory
739. Massachusetts Institute of Technology
Att: Librarian
740. McDonnell Aircraft
Att: Librarian
741-742. MSA Research Corporation
Att: Librarian, R. C. Andrews
743. North American Aviation, Inc.
Att: Librarian
744. Pratt and Whitney Aircraft Corporation
Att: Librarian
745-747. Pratt and Whitney Aircraft, CANEL
Att: Librarian, K. J. Kelly, Robert Strouth
748. Republic Aviation Corporation
Att: Librarian
749. Rocketdyne
Att: Librarian
750. Solar
Att: Librarian
751. Southwest Research Institute
Att: Librarian
752. Sylvania Electric Products, Inc.
Att: Librarian
753. Temescal Metallurgical
Att: Librarian
754. Union Carbide Metals
Att: Librarian
755. United Nuclear Corporation
Att: Albert Weinstein
756. University of Michigan
Att: Librarian
757. Vought Astronautics
Att: Librarian
758. Westinghouse Electric Corporation, Aerospace Department
Att: Librarian
759. Westinghouse Electric Corporation, Astronuclear Laboratory